Int. J. Electrochem. Sci., 7 **(2012)** 8151 - 8169

International Journal of
ELECTROCHEMICAL
SCIENCE
www.electrochemsci.org

Electroless Synthesis of Ni-P and Ni-P-Zn Alloy Coatings for Protecting Steel Rebar from Chloride-Induced Corrosion

Yongxin Li[1, 2], *Prathish Kumar*[1], *Xianming Shi*[4, 1, 5,*], *Tuan Anh Nguyen*[1], *Zhenjian Xiao*[3], *Jianlin Wu*[4]

[1] Corrosion and Sustainable Infrastructure Laboratory, Western Transportation Institute, PO Box 174250, College of Engineering, Montana State University, Bozeman, MT 59717-4250, USA
[2] College of Chemistry and Materials Science, Anhui Normal University, Wuhu 241000, China
[3] Shenzhen Jinzhou Precision Technology Corp., Longgang High-Tech Industry Park, Shenzhen 518116 , China.
[4] School of Civil Engineering and Architecture, Wuhan Polytechnic University, Wuhan, 430023, China.
[5] Civil Engineering Department, 205 Cobleigh Hall, Montana State University, Bozeman, MT 59717-2220, USA
[*]E-mail: xianming_s@coe.montana.edu

Received: 13 July 2012 / *Accepted:* 3 August 2012 / *Published:* 1 September 2012

Ni-P based alloy coatings on the surface of carbon steel were prepared by electroless deposition method and their microstructure, chemistry and corrosion behaviors were investigated using scanning electron microscope (SEM), energy dispersive X-ray (EDX), linear polarization, cyclic voltammetry and electrochemical noise techniques, respectively. The bath solution chemistry was found to play a significant role in the microstructure and properties of the electroless Ni-P and Ni-P-Zn coatings. With a dense and homogeneous surface microstructure, the best Ni-P coating featured corrosion behavior nearly comparable to 304 stainless steel coupons in neutral 3% NaCl. The cyclic voltammetry measurements indicated positive risks of localized corrosion (either crevice corrosion or pitting) for the bare steel rebar (ASTM A615) and all the Ni-P and Ni-P-Zn coatings tested considerably reduced such risks. The corrosion behavior of the selected coatings or bare steel rebars was determined by exposing the rebars in a Simulated Pore Solution (SPS) at pH 13.6 with 1 wt% NaCl media for up to 72 h. The electrochemical noise measurements showed that the corrosion resistance of Ni-P coating and Ni-P-Zn coating were significantly higher than that of bare steel rebar in the basic and salty environment. On average, they featured corrosion protection against chloride-induced corrosion nearly to the level of protection by 316 stainless steel. These alloy coatings provided enhanced corrosion protection for the commercially available steel rebar; as such, they show great promise as an effective and convenient way of treating steel rebars for concrete applications.

Keywords: Ni-P; Ni-P-Zn; Electrochemical noise; Corrosion rate; Steel rebar

1. INTRODUCTION

Cementitious materials such as concrete and mortar are extensively used in ports, buildings, bridges and roads, which are often reinforced by metallic rebars. While the alkaline pore solution (pH > 12.5) in cementitious materials generally protects the rebar from degradation, cementitious materials feature heterogeneity and relatively high permeability. As such, the ingress of deleterious ionic species such as chloride, once exceed certain thresholds, can result in the disruption of the rebar's passive film and initiate its localized corrosion [1-3]. The chloride-induced rebar corrosion is one of the major risks for the durability, serviceability and reliability of reinforced concrete structures [4-8]. To mitigate this risk and extend the service life of reinforced concrete, anti-corrosion coatings, corrosion inhibitors, electrochemical protection or rehabilitation are the common measures explored by researchers and practitioners worldwide [9-14]. Among them, treating the rebar surface with an electroless coating is one convenient yet underexplored way for enhancing the corrosion resistance of rebar in concrete.

Ni alloys and stainless steels may be used as corrosion-resistant rebars. Their high cost, however, make them less attractive for reinforced concrete applications. As such, treating commonly available, inexpensive carbon steel rebars with a Ni alloy coating holds the promise for a cost-effective solution to chloride-induced corrosion [15]. Usually, two methods can be used to fabricate Ni alloy coating: electrodeposition and electroless deposition. For electrodeposition, the formation of a uniform Ni alloy coating on the rebar surface is difficult to achieve, considering the presence of ribs at regular interval on the rebar surface [12]. In contrast, electroless Ni-based coatings are finding increased use in a diverse variety of applications in chemical, food, and automotive industries, since this technology can be utilized to synthesize uniform coatings with excellent chemical and mechanical properties [16]. Electroless Ni-based coatings have been reported to feature good anti-corrosion and wear resistance properties [17, 18]. The reduction of nickel ions in the presence of sodium hypophosphite (NaH_2PO_2) can produce an alloy of nickel and phosphorus [19]. The Ni and P contents in the alloy coating are governed by the composition, temperature and the pH of the plating bath used [20, 21]. Many studies have attempted to understand the characteristics of deposition process of Ni-P and Ni-P-Zn alloys. Flis and Duquette [22] evaluated Ni-P alloys in near-neutral and alkaline solutions and found both beneficial and detrimental effects depending upon the amount of P content in the coating. Abdel Hamid et al. [12] found that codeposition of Zn with Ni-P could improve the corrosion resistance in an alkaline solution (pH 9.5).

For the evaluation of anti-corrosion performance of metallic coatings, most measurements are based on electrochemical methods such as linear polarization, cyclic voltammetry, and electrochemical impedance spectroscopy. Electrochemical noise analysis (ENA) is a relatively underutilized technique, which monitors and analyzes potential and current fluctuations spontaneously generated by corrosion reactions over time. Relative to other electrochemical methods, ENA does not pose any external disturbance to the corrosion behavior of metallic coating to be characterized and thus is inherently non-destructive and non-disruptive [23, 24]. As such, it has been increasingly used to investigate corrosion processes in the past two decades [25-27]. ENA has been reported to enable the detection and

differentiation of different corrosion types [28, 29] and to allow the detection and evaluation of corrosion activities.

In this work, Ni-P and Ni-P-Zn alloy coatings were developed on carbon steel surfaces via electroless deposition. The effect of bath solution chemistry on the surface morphology and corrosion resistance of the electroless coatings in 3% NaCl was explored. Subsequently, the study focused on a few selected bath solutions to deposit Ni-P or Ni-P-Zn coatings on steel rebars. The anti-corrosion performance of these coatings in a chloride-containing simulated concrete pore solution was evaluated using ENA as well as linear polarization and cyclic voltammetry measurements.

2. EXPERIMENTAL

2.1. Materials

Table 1. Preliminary study: bath solution chemistry and average roughness of electroless coatings on steel rebar.

Bath Solution	Ni-P Coating		
	pH=5 (NH_3(aq))	pH 5 (NaOH)	pH 5 (H_3PO_4)
	$NaH_2PO_2.H_2O$ 5-24 g/L	$NaH_2PO_2.H_2O$ 26.5-53 g/L	53 g/L
	$NiSO_4 \cdot 6H_2O$ 5-32 g/L	$NiCl_2.6H_2O$ 23.8-71.3 g/L	35.7-47.5 g/L
	CH3CH(OH)COOH 14-56 g/L	$(NaOOCCH_2\text{-})_2 \cdot 6H_2O$ 27-40.5 g/L	40.5 g/L
	CH_3CH_2COOH 1.1-4.4 g/L	-	-
	$Pb(NO_3)_2$ 1-2 ppm	-	-
Average Roughness R_a (μm)	0.18-1.33	0.38-6.08	0.10-0.62
Bath Solution	Ni-P-Zn Coating		
	pH=7 (NH3(aq))	pH 7 (NaOH)	pH 7 (H_3PO_4)
	$NaH_2PO_2.H_2O$ 2-10 g/L	3-45 g/L	2-8 g/L
	NiCl2.6H2O 6-10 g/L	6-47.5 g/L	8 g/L
	Citric Acid 10-30 g/L	4-20 g/L	10-15 g/L
	NH_4Cl 5-13 g/L	10-26 g/L	5-8 g/L
	$ZnCl_2$ 4-6 g/L	4-8 g/L	4-6 g/L
Average Roughness R_a (μm)	0.004-0.032	0.10-0.39	0.01-0.03

The steel rebars used in this research were obtained from Bozeman Metal (Bozeman, MT) with a diameter of 3/8 inches (1 cm). The specimens were cut from Nucor Steel-Utah 10/#3 Rebar 20’2K (ASTM A615/A615M-09 GR 40) to be 15 cm in length. The chemical composition of the rebar was

(in wt. %): 0.16% C; 0.22% Si; 0.72% Mn; 0.043% Mo; 0.3% Cu; 0.041% S; 0.014% P; 0.014% Ni; 0.22% Cr. The steel coupons used in this research purchased from Metal Samples (Munford, AL) were of Cor-ten B type (ASTM A588/UNS #K11430; density: 7.60 g/cm^3; chemical composition: C 0.10 – 0.19 %, Si 0.15 – 0.30 %, Mn 0.90 – 1.25 %, Cu 0.25 – 0.40 %, S ≤ 0.05 %, P ≤ 0.04 %, Cr 0.40 – 0.65 %, V 0.02 – 0.10 %, Fe 97.0 – 98.2 %) with the exposed surface area of 2 cm^2.

Sodium chloride (NaCl) and other chemicals used were purchased from Fisher Scientific (Pittsburgh, PA). A simulated pore solution (SPS) of pH 13.6 was prepared and added with 1 % NaCl to create a corrosive solution simulating the salt-contaminated concrete environment. This is to maintain the [Cl^-]/[OH^-] ratio of 0.43, which slightly exceeds the typical chloride threshold level for rebar corrosion in concrete [30].

Table 2. Bath solution chemistry for the in-depth study of electroless Ni-P and Ni-P-Zn coatings on steel rebar, with pH adjusted to 5.0 and 7.0 respectively using NH_3(aq).

Chemicals (g/L)	Ni-P coatings				Chemicals (g/L)	Ni-P-Zn coatings			
	#1	#2	#3	#4		#5	#6	#7	#8
$NiSO_4 \cdot 6H_2O$	21	30	21	21	$NiSO_4 \cdot 6H_2O$	21	21	21	21
$NaH_2PO_2.H_2O$	24	24	30	40	$NaH_2PO_2.H_2O$	24	24	24	30
CH3CH(OH)COOH	14	14	14	14	Citric Acid	10	10	10	10
CH_3CH_2COOH	2.2	2.2	2.2	2.2	$ZnCl_2$	6	4	8	6
$Pb(NO_3)_2$ (ppm)	1	1	1	1	$Pb(NO_3)_2$ (ppm)	1	1	1	1

2.2. Preparation of Samples.

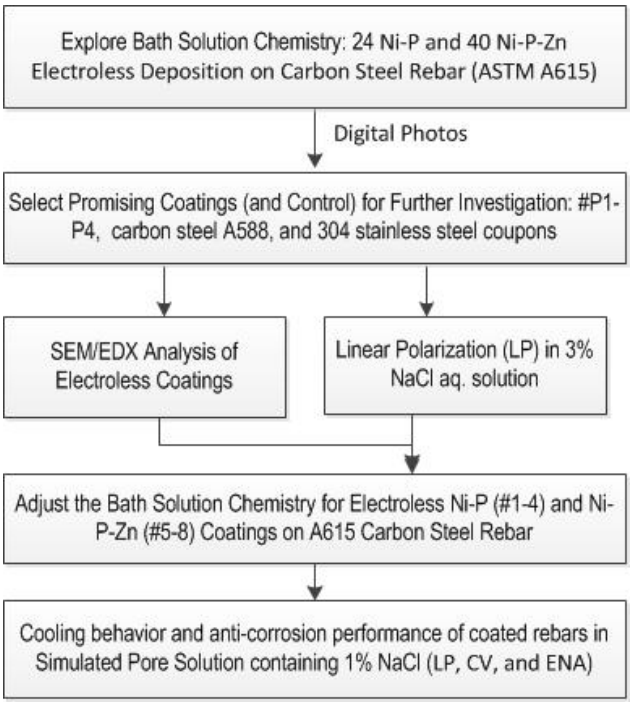

Figure 1. Schematic experimental plan for the characterization of steel rebars or coupons.

The steel rebars and coupons were polished using different grades of SiC sandpaper up to # 1000 to remove any rust that had formed on their surface. Subsequently, they were cleaned with de-ionized (DI) water and dried before being used in this study. Prior to coating the rebars and coupons they were dipped in a solution of 5% HCl for 30 seconds and rinsed with DI water, which aimed to activate the steel substrates to be coated. For the preliminary study and in-depth study detailed later, their bath solution chemistry for the electroless coatings is detailed in Table 1 and Table 2, respectively.

Once the bath solution reached 85°C, the rebars or coupons which had been acid-treated were placed inside the solution for 1 hr to allow electroless deposition of Ni-P or Ni-P-Zn on them. Subsequently, they were rinsed with DI water, before being heated for post-treatment. The post-treatment for the preliminary study and in-depth study was 200°C/2hr and 350°C/1hr, respectively. For the in-depth study, the cooling rates of the heated samples were recorded.

2.3. Characterization of Steel Rebars or Coupons

Fig. 1 shows the flowchart of steps taken to test the properties of bar steel and steel coated with Ni-P or Ni-P-Zn, in the effort to identify the best-performing anti-corrosion alloy coating for treating steel rebar. A preliminary study of electroless coatings for steel rebars was first conducted, by exploring the effects of bath solution chemistry (24 Ni-P coatings and 40 Ni-P-Zn coatings respectively). The micro-roughness of the coated surfaces was characterized using a hand-held roughness tester (Model TR200, Time Group Inc., Beijing, China) with cut-off length of 0.25 mm to 2.5 mm. The parameter R_a was used to describe the surface roughness, which is a common way of quantifying the height variations of a given surface. R_a is the arithmetic mean of the absolute value of profile derivation from the mean within sampling length. For this study, the portable tester was used to measure at minimum three 0.8×5 mm^2 areas, from which an average R_a value was calculated. Furthermore, the resulted surface morphology was assessed from digital photos (as illustrated in Fig. S1 in *Supplementary data*) and 4 bath solutions leading to coatings with relatively uniform top surface were selected to deposit coatings on steel coupons.

These select coatings were then analyzed by field emission scanning electron microscopy and energy-dispersive x-ray spectroscopy (FESEM/EDX), which unravel the coating's localized morphology and elemental distributions at the microscopic level respectively. For this study, we used a Zeiss Supra 55VP PGT/HKL system (Hitachi S-4100, Japan) coupled with the EDX analyzer under variable pressure (VP mode), typically 10−2 torr. The EDX data were obtained with a micro-analytical unit that featured the ability to detect the small variations of trace element content. These select coatings were also evaluated for their anti-corrosion performance in 3% NaCl solution using linear polarization.

In light of the findings from the preliminary study, the bath solution chemistry was further adjusted to deposit 4 Ni-P and 4 Ni-P-Zn coatings on steel rebars, respectively. The anti-corrosion performance of these 8 metallic coatings was individually assessed in the chloride-containing SPS using linear polarization, cyclic voltammetry and ENA, with the bare steel rebar as control.

2.3.1. Linear Polarization and Cyclic Voltammetry Measurements

The electrochemical tests were conducted with a Gamry Potentiostat model Reference 600 (Gamry Instruments, PA, US) with a traditional three-electrode system, consisting of a platinum mesh as counter electrode, a saturated calomel electrode (SCE) as reference electrode and the bare or coated steel rebars as working electrode. For the preliminary study of electroless coatings, the steel rebars were immersed in 3% NaCl aqueous solution for 24 h, with the corrosion potential (E_{corr}) and linear polarization (LP) measurements conducted at 1hr and 20 hr, respectively. For the in-depth study of select electroless coatings, the steel rebars were immersed in the SPS solution with 1% NaCl for 24 h prior to the electrochemical tests. The LP measurements were conducted at ± 20 mV around its open circuit potential (OCP) by a direct current (DC) signal around its open circuit potential (OCP), at a scan rate of 0.2 mV/s. The cyclic voltammetry (CV) measurements were conducted at a scan rate of 12 mV/s, with the scan range between -0.6 V/SCE to + 0.6 V/SCE.

2.3.2. Electrochemical Noise Measurements

Electrochemical noise data were obtained using a Gamry Instrument Reference 600. The mode of the program used to measure the data was zero resistance ammeter (ZRA) at a scan rate of 1 Hz. The ZRA method uses three electrodes including two identical rebars as working electrodes and a SCE as reference electrode. The experiment was conducted at ambient conditions in a Faradays cage (shown in Fig. S2 in *Supplementary data*). Note that the Faradays cage also covered two beakers containing DI water around the test apparatus, which aimed to minimize any evaporation from the test solution. The rebars were immersed in the 1% NaCl + SPS solution for 72 h, during which the potential and current between the two rebars were monitored.

2.4. Data analysis

2.4.1 Electrochemical Noise Analysis (ENA)

ENA was performed in time and frequency domains using the ESA 400 software provided by Gamry Instrument (ESA 400). For each select coating and the control (bare steel), three duplicates were tested. The analysis in the time domain provides the mean values of the potential *E* vs. SCE, the noise resistance R_n as well as the Localized Index *LI* (following Equation 1) [31].

$$LI = \frac{\sigma I}{rmsI} \qquad (1)$$

In Equation 1, *rmsl* indicates the electrical current fluctuation and σI is the variance in electrical current. *LI* can also be defined as follows [31]:

$$LI = \sqrt{\frac{\sum_{i=1}^{N}(x_i - \tilde{x})^2}{\sum_{i=1}^{N} x_i^{\,2}}} \qquad (2)$$

The ESA 400 software also provides the skewness *S* and kurtosis *k*. These two parameters characterize the shape distribution of the data.

$$S = \frac{1}{N}\sum_{i=1}^{N}\left(\frac{x_i - \tilde{x}}{\sigma}\right)^3 \quad (3)$$

$$k = \frac{1}{N}\sum_{i=1}^{N}\left(\frac{x_i - \tilde{x}}{\sigma}\right)^4 \quad (4)$$

When $k = 3$, this indicates a normal distribution; when $k > 3$, the distribution is more sharply peaked and $k < 3$ indicates flat topped [31]. The electrochemical noise also provides three other parameters: I_{corr} is the average corrosion current, q is the average charge of each event, and f_n is the frequency of events.

$$I_{corr} = qf_n \quad (5)$$

$$q = \frac{\sigma_1 \sigma_E}{Bb} \quad (6)$$

$$f_n = \frac{I_{corr}}{q} = \frac{B^2 b}{\sigma_E{}^2} \quad (7)$$

$$R_n = \frac{\sigma_E}{\sigma_I} \quad (8)$$

Note that σ_I and σ_E in Equations 6 and 7 are the standard deviations of electrical current and potential. *B* and *b* are the Stern–Geary coefficient and bandwidth measurement, respectively. The R_n value in Equation 8 is calculated from time-domain analysis and can be directly related to the polarization resistance R_p [32].

2.4.2 Linear Polarization and Cyclic Voltammetry Analyses

In order to find which composition of bath solution provides the best corrosion protection, both LP and CV techniques were employed for evaluating the select electroless coatings. For each select coating and the control (bare steel), three duplicate experiments were run. The LP analysis can give two important parameters characterizing the corrosion behavior of metallic coatings, E_{corr} and R_p. It is well-known that $1/R_n$ is proportional to the corrosion rate (I_{corr}), as defined in Equation 9, which is the

Stern-Geary equation. β_a , β_c in Equation 10 are the anodic and cathodic Tafel constant, respectively [33].

$$I_{corr} = \frac{B}{R_p} \quad (9)$$

$$B = \frac{\beta_a \beta_c}{2.3(\beta_a + \beta_c)} \quad (10)$$

For both bare steel and Ni-based coatings, the value of β_a and β_c were taken to be 0.12 *V/Decade*, this gives the value of B = 0.026 V. Previous studies have shown that this simplification does not significantly affect the calculation of corrosion rate [34].

The CV analysis can give several important parameters characterizing the anti-corrosion performance of metallic coatings, such as corrosion current density (I_{corr}), R_p, corrosion potential (E_{corr}), pitting potential (E_{pit}), and repassivation potential (E_{rep}). Note that CV is a destructive test since the amount of polarization to the working electrode of interest is high. Based on unpublished data from our lab, the thermodynamic parameters (i.e., potentials) are much more reproducible than the kinetic parameters (I_{corr} and R_p). As such, we only used E_{corr}, E_{pit}, and E_{rep} as key parameters derived from the CV data of this study.

3. RESULTS AND DISCUSSION

3.1. Effects of Bath Solution Chemistry - Preliminary Exploration

The section is concerned with exploring the effect of bath solution chemistry on the quality of synthesized Ni-P or Ni-P-Zn coating on the steel rebars. As summarized in Table 1, the preliminary study evaluated a total of 24 bath solutions for depositing Ni-P coatings on the steel rebars, 14, 6 and 4 of which used NH_3(aq), NaOH and H_3PO_4 respectively to adjust to pH 5.0. In addition, the preliminary study evaluated a total of 40 bath solutions for depositing Ni-P-Zn coatings on the steel rebars, 9, 14 and 17 of which used NH_3(aq), NaOH and H_3PO_4 respectively to adjust to pH 7.0. As illustrated by the rebars numbered as P1, P2, and P3 (Fig. S1 in *Supplementary data*), the bath solution chemistry considerably affected the surface morphology of Ni-P coatings formed on the ASTM A615 carbon steel substrate. In contrast, the effect of bath solution on the surface morphology of Ni-P-Zn coatings was also significant but not as dramatic. These observations are consistent with the diversity seen in the surface micro-roughness (R_a values in Table 1). Note that most coated steel rebars showing apparently non-uniform surface morphology were excluded from further investigation.

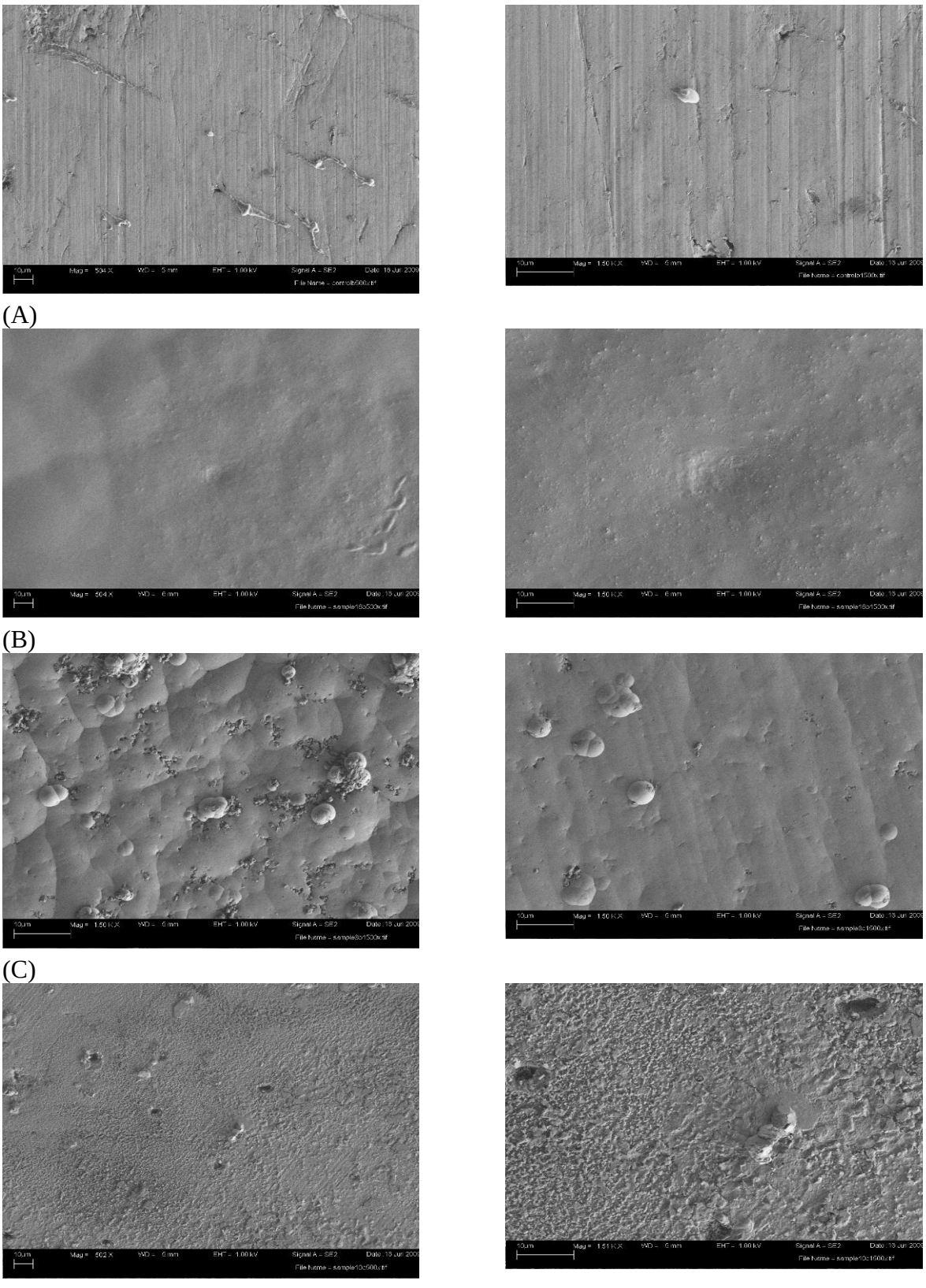

Figure 2. SEM micrographs of bare and coated steel rebar surfaces. (A) bare A615 carbon steel; (B) good Ni-P coating (#P2); (C): poor Ni-P coating (#P3); (D) worst Ni-P-Zn coating (#P4). Left: 500× magnification; right: 1,510 × magnification.

To explore the microstructure, composition and performance of representative coatings, 4 bath solutions leading to coatings with relatively uniform top surface (#P1, P2, P3 and P4) were selected to deposit coatings on steel coupons. These select coatings were then analyzed by FESEM and EDX, which unravel the coating's localized morphology (Fig. 2) and elemental distributions (Table S1 in *Supplementary data*) at the microscopic level respectively. From Fig. 2A, it can be seen that some scratches and residual contaminants remained on the bare carbon steel coupon. These defects from the polishing process are typical and may provide localized sites for corrosion to initiate in natural environment [35, 36]. At both micron and sub-micron scales, the good Ni-P coating ((#P2) featured very dense and homogeneous surface microstructure whereas the poor Ni-P coating (#P3) exhibited dense yet heterogeneous microstructure. In contrast, the worst Ni-P-Zn coating (#P4) exhibited very loose deposition of particles and the presence of submicron cracks in the deposited surface layer. The data in Table S1 (see *Supplementary data*) also reveal that the electroless deposition of Ni-P-Zn coating (#P4) on the ASTM A588 carbon steel substrate was unsuccessful, since the surface layer was still dominated by the Fe element instead of Ni. This failure to cover the steel substrate with a dense Ni-P-Zn coating [37] is attributed to the specific bath solution used for electroless deposition. On the other hand, the electroless deposition of Ni-P coatings (#P2 and P3) was successful, since the surface layer was dominated by the Ni element instead of Fe.

Table 3. Bath solution chemistry and corrosion performance in 3% NaCl (with bare carbon steel A588 and bare stainless steel 304 SS as control).

	Ni-P Coating			Ni-P-Zn Coating	A588	304 SS
	#P1	#P2	#P3	#P4		
	pH=5 (NH3(aq))	pH=5 (NH3(aq))	pH 5 (NaOH)	pH 7 (NaOH)		
Bath Solution	$NaH_2PO_2.H_2O$ 24 g/L	24 g/L	53 g/L	4 g/L	NA	
	$NiSO_4 \cdot 6H_2O$ 21 g/L	21 g/L	$NiCl_2.6H_2O$ 35.7 g/L	8 g/L		
	CH3CH(OH)COOH 56 g/L	14 g/L	$(NaOOCCH_2-)_2 \cdot 6H_2O$ 40.5 g/L	Citric Acid 20 g/L		
	CH_3CH_2COOH 4.4 g/L	2.2 g/L	-	NH_4Cl 13 g/L		
	$Pb(NO_3)_2$ 2 ppm	1 ppm	-	$ZnCl_2$ 6 g/L		
Average Roughness R_a (µm)	0.18	0.40	6.08	0.39	0.17	0.035
Corrosion Rate @ 1hr (MPY)	0.30	0.070	0.04	3.51	3.25	0.0038
E_{corr} (mV, vs. SCE) @ 1hr	-387	-356	-340	-538	-515	-170
Corrosion Rate @ 20hr (MPY)	2.50	0.0048	0.06	5.54	2.56	0.0030
E_{corr} (mV, vs. SCE) @ 20hr	-583	-217	-366	-694	-739	-71

These select coatings were also evaluated for their anti-corrosion performance in 3% NaCl solution using linear polarization measurements at 1 hr and 20 hr of immersion. As shown in Table 3, the worst Ni-P-Zn coating (#P4) on the ASTM A588 carbon steel substrate slightly altered its corrosion potential and slighted accelerated its corrosion in 3% NaCl. In comparison, the electroless Ni-P coatings significantly modified the ASTM A588 carbon steel substrate, shifted its corrosion potential to the noble direction, and greatly reduced its corrosion in 3% NaCl. Among the three Ni-P coatings investigated, the best one (#P2) tended to lead to the highest corrosion potential and lowest corrosion rates, likely due to the formation of nano- and micro-crystalline deposits [38]. The Ni-P coatings reduced the number of defect sites on the steel surface and substantially modified the metal/electrolyte interface. It is noteworthy that the best Ni-P coating (#P2) featured corrosion behavior nearly comparable to 304 stainless steel coupons. The superior corrosion resistance of Ni-P coatings #P2 to #P3 can be attributed to its dense and homogeneous surface microstructure (as shown in Fig. 2) and its desirable chemical composition (indicated by higher Ni/Fe and P/Ni ratios shown in Table S1 in *Supplementary data*). Our unpublished data also indicate that Ni-P and Ni-P-Zn coatings greatly improved the thermal conductivity of steel substrate, which may have implications for engineering applications (e.g., high-temperature corrosion).

3.2. Cyclic Voltammograms of Bare and Coated Steel Rebars

The anti-corrosion performance of the 8 select alloy coatings was individually assessed in the chloride-containing SPS using linear polarization (LP) and cyclic voltammetry (CV) measurements, with the bare steel rebar as control.

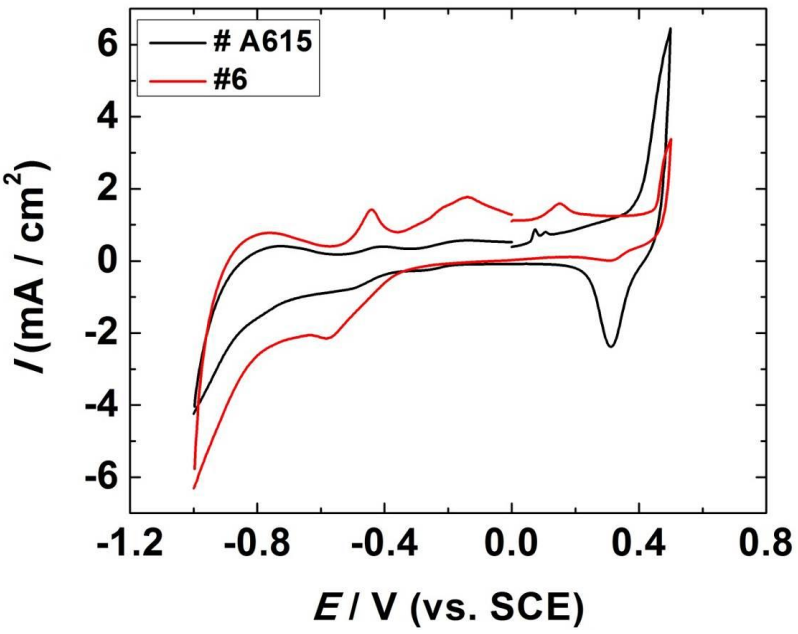

Figure 3. Cyclic voltammograms for the bare steel rebar (A615) and that coated by Ni-P-Zn (#6).

For each rebar, its corrosion potential was derived from the LP measurement whereas its pitting potential (E_{pit}) and repassivation potential (E_{rep}) of the steel rebar was derived from the CV measurement [38]. Based on linear polarization resistance measured, #3 and #6 were considered to be the best-performing Ni-P coating and Ni-P-Zn coating, respectively, among the alloy coatings investigated. Thereafter, the surface morphology of these two coatings were examined using SEM and found to be very similar to those seen in Fig. 2B, i.e. featuring very dense and homogeneous surface microstructure.

Fig. 3 provides good contrast between the cyclic voltammogram of bare steel rebar (A615) and that of a steel rebar coated by Ni-P-Zn (#6). In this work, E_{pit} is defined as the potential in the anodic scan beyond which the current density increases notably and rapidly above the passive current density, and E_{rep} is defined as the potential in the cathodic scan beyond which the current density decreases notably and rapidly below the passive current density. As shown in Figure 5, the Ni-P-Zn coating significantly increased both E_{pit} and E_{rep} of on the carbon steel substrate and considerably reduced its pitting current density, all of which suggest enhanced resistance to localized corrosion.

For the bare steel rebar, its CV plot featured a clear range of "passive" electrochemical potentials in which the current density remained small and nearly independent of the applied potential. For the rebars with Ni-P or Ni-P-Zn coatings, however, their current density in the "passive" zone featured more variations, likely attributable to the selective changes in the coating's chemical composition as a function of the applied potential. For the CV plot of coated rebars, the current in the cathodic scan greatly deviated from its counterpart in the corresponding anodic scan, further suggesting the presence of localized chemical changes.

Table 4. Average electrochemical potential data obtained from the CV measurements of carbon steel (ASTM A615) and carbon steel protected by Ni-P based coatings.

Ni-P	$E_{corr} - E_{pit}$ (mV)	$E_{corr} - E_{rep}$ (mV)	Ni-P-Zn	$E_{corr} - E_{pit}$ (mV)	$E_{corr} - E_{rep}$ (mV)
#1	-143.3	-109.8	#5	-190.8	-100.0
#2	-242.1	-121.1	#6	-132.2	-54.2
#3	-261.4	-168.0	#7	-200.7	-55.4
#4	-185.0	-110.1	#8	-242.2	-82.6
Uncoated A615	5.5	66.0	Uncoated A615	5.5	66.0

The susceptibility of steel rebars to pitting corrosion and crevice corrosion in the basic and salty environment can be quantitatively characterized by ($E_{corr} - E_{pit}$) and ($E_{corr} - E_{rep}$), respectively [30]. As shown in Table 4, under the investigated conditions, there are positive risks of localized corrosion (either crevice corrosion or pitting) for the bare steel rebar and all the Ni-P and Ni-P-Zn coatings considerably reduced such risks. Note that both LP and CV data ranked #3 as the best-

performing Ni-P coating, whereas they disagreed on the ranking of #6 as the best-performing Ni-P-Zn coating.

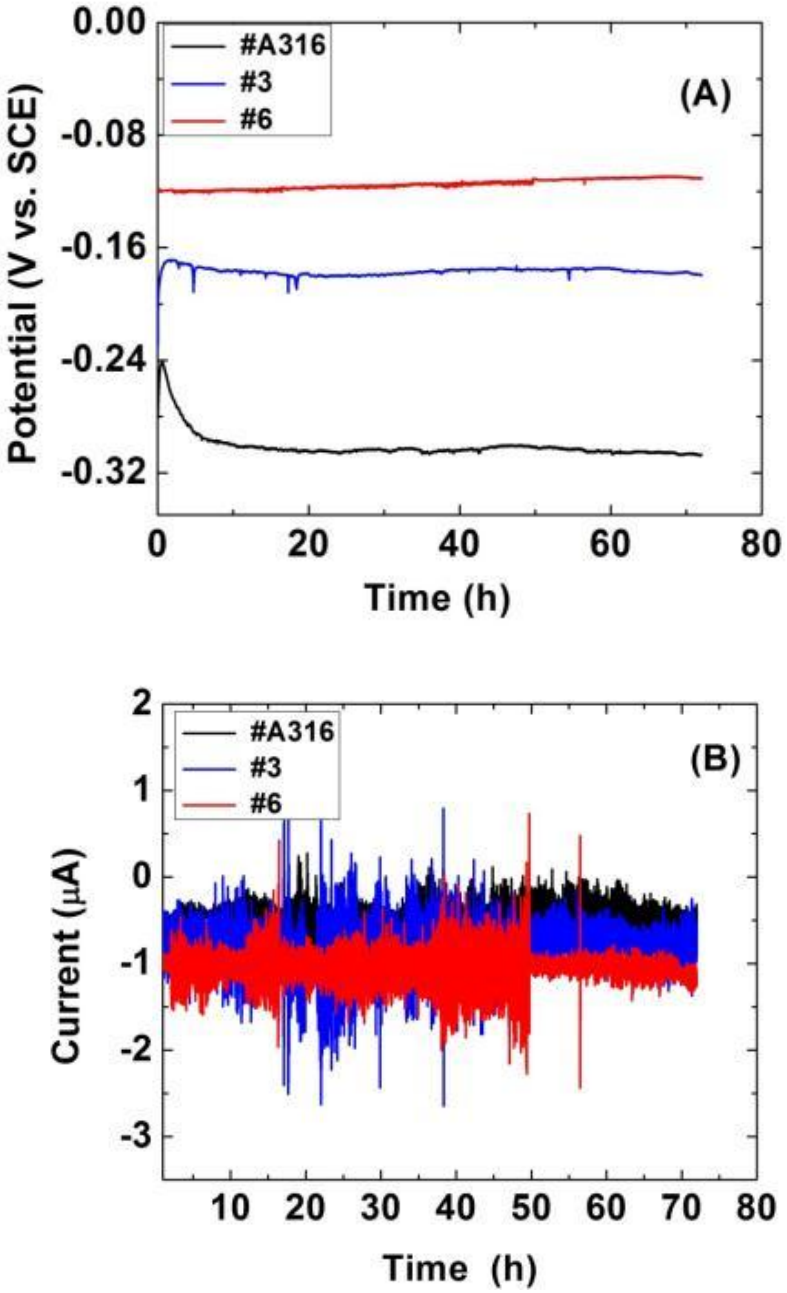

Figure 4. Temporal evolution of potential (A) and current (B) for the stainless steel rebars (A316, black curve), Ni-P coating rebars (#3, blue curve) and Ni-P-Zn coating rebars (#6, red curve) while undergoing corrosion in the reaction cell for 72 h.

3.3. Electrochemical Noise Measurements of Bare and Coated Steel Rebars

The section is concerned with exploring the use of ENA for assessing the anti-corrosion performance of the best-performing Ni-P (#3) and Ni-P-Zn (#6) coatings. The potential noise and current noise over time were measured in the freely-corroding system as described in the experimental

section. All the tested rebars exhibited distinctive fingerprint-like patterns in their temporal evolution of potential and current between two identical rebars, as shown in Fig. 4. From Fig. 4A, it can be seen that the values of potential noise in the 1% NaCl + SPS solution followed the order of $E_{\text{Ni-P-Zn}}$ (-0.12 V) > $E_{\text{Ni-P}}$ (-0.17 V) > $E_{\text{stainless steel}}$ (-0.31 V), suggesting the significant difference in the metal/electrolyte interfaces of the three systems. From Fig. 4B, it can be seen that for all three types of rebars, their current noise fluctuated greatly during the first 50 h and then remained somewhat stable thereafter. This implies strong interaction between the rebar surface (either bar stainless steel or alloy-coated carbon steel) and the NaCl-containing SPS solution during the first phase and potential formation and stabilization of passive film during the second phase.

Table 5. Electrochemical noise resistance, corrosion current, charge, localized index and corrosion rate values for bare carbon steel rebars (A615), stainless steel rebars (A316), Ni-P coated rebars (#3), and Ni-P-Zn coated rebars (#6) in the reaction cell for 72 h.

Samples	R_n (kΩ)	I_{corr} (μA)	q(μC)	LI	MPY
A615	7.78	3.35	8.74	0.073	0.169
A316	69.80	0.38	0.03	0.094	0.019
Ni-P (#3)	101.05	0.27	0.08	0.181	0.013
Ni-P-Zn (#6)	109.30	0.24	0.21	0.276	0.012

The electrochemical noise data were analyzed in the time domain, following Equations 1 to 8. This led to the values of noise resistance (R_n), Localized Index (*LI*), corrosion current (I_{corr}), transfer charge (q), and corrosion rate (in milli-inches per year or MPY), as presented in Table 5. One can conclude from R_n, I_{corr}, and corrosion rate data that on average, the carbon steel rebars coated by the Ni-P-Zn (#6) featured the highest noise resistance and lowest corrosion rate over the 72-h exposure, followed by the carbon steel rebars coated by the Ni-P (#3) and then the 316 stainless steel rebars. Such outstanding corrosion resistance of the Ni-P and Ni-P-Zn coatings may be attributed to the formation of phase structure and/or nano- and micro-crystalline deposits [38, 40]. In this specific case, codeposition of Zn with Ni-P did not significantly improve the corrosion resistance in an alkaline solution, which differs from the case reported in literature [12]. As demonstrated in this work, even a small change in the ionic concentrations of bath solution may result in significant change in the properties of the deposited alloy coating. As such, enhanced anti-corrosion performance of Ni-P-based coatings can be expected from improvements made to the bath solution and/or the electroless deposition and post-treatment parameters. From the q data, one can conclude that the stainless steel rebars featured the lowest average charge per corrosion event, followed by the carbon steel rebars coated by the Ni-P (#3) and then those coated by the Ni-P-Zn (#6). It is interesting to note that the bare carbon steel rebars (A615) featured q one to two orders of magnitude higher than the more corrosion-resistant rebars, suggesting fundamentally different types of corrosion events on their surface (i.e., macro-events vs. micro-events). This also confirms that the Ni-P and Ni-P-Zn coatings greatly enhanced the corrosion resistance of the carbon steel substrate. *LI* can have values between 0 and 1, with 0 and 1 being characteristic of uniform corrosion and localized corrosion, respectively. From the

LI data, one can conclude that the prevailing corrosion mechanism for both bare carbon steel and stainless steel rebars was uniform corrosion. While that remains true for the carbon steel rebars coated with Ni-P or Ni-P-Zn, their probability to corrode in a localized fashion (if corrosion initiates) is somewhat significant. This is not in disagreement with the fact that they feature higher resistance to corrosion and lower susceptibility to localized corrosion. The *q* and *LI* data together can be used to manifest the nature of the transient corrosion events on the surface of the metal or alloy.

Power spectrum density (PSD), describing how the power (or variance) with time series is distributed with frequency, is a useful tool in assessing the frequency dependence of electrochemical noise data [41, 42]. Fig. 5 presents the traditional fast Fourier transform (FFT) analysis of electrochemical noise collected from the stainless steel rebars, Ni-P coated steel rebars, and Ni-P-Zn coated steel rebars. For all three systems, their power spectrum density (PSD) of both potential and current noise data decreased with the frequency and the logarithm of the two generally followed a linear trend. According to Uruchurtu et al., the roll-off slope of PSD much lower than -20 dB dec^{-1} symbolizes uniform corrosion [43]. The values of the roll-off slope of PSD shown in Fig. 5 and Table 6 are much higher than -20 dB dec^{-1}, suggesting that the prevailing nature of corrosion on the rebar surfaces was localized corrosion (vs. uniform corrosion).

Table 6. Average slope values and average Y-intercept for carbon steel rebars (A615), stainless steel rebars (A316), Ni-P coated rebars (#3), and Ni-P-Zn coated rebars (#6) in the reaction cell for 72 h.

Samples	Avg. Slope (dB dec^{-1})	Avg. Y-int. log ($\Omega.cm^2$)
A615	-1.11	1.69
A316	-0.54	2.48
Ni-P (#3)	-0.86	1.71
Ni-P-Zn (#6)	-0.79	1.95

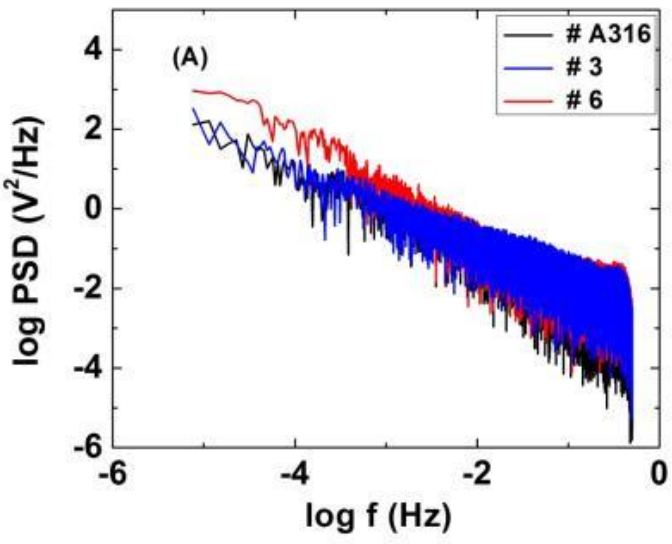

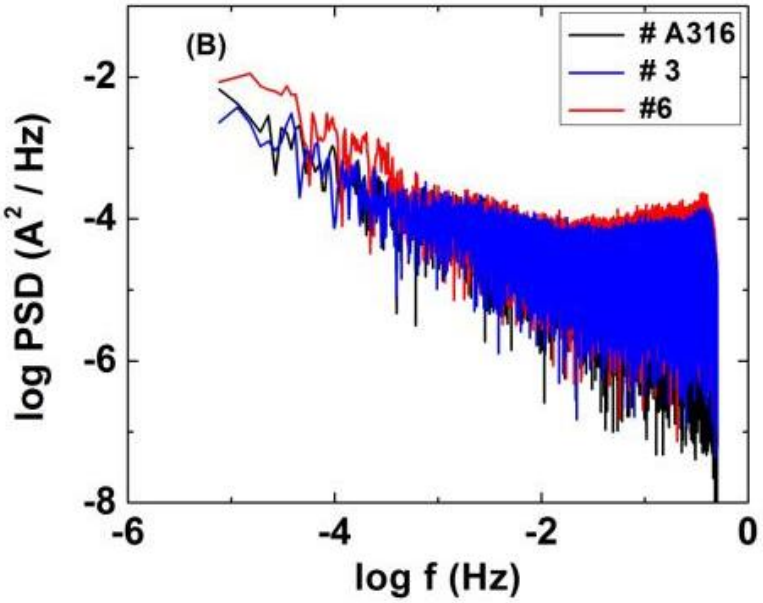

Figure 5. PSD analysis for the stainless steel rebars (A316, black curve), Ni-P coated steel rebars (#3, blue curve) and Ni-P-Zn coated steel rebars (#6, red curve): (A) potential noise; (B) current noise.

As shown by both the slope and intercept data in Table 6, the PSD results suggest that the corrosion resistance of the carbon steel rebars coated by Ni-P or Ni-P-Zn coatings to be higher than bare carbon steel rebars (A615) but lower than stainless steel rebars (A316). Compared with the ENA in the time domain, the anti-corrosion performance of Ni-P-based coatings (relative to 316 stainless steel) was less impressive based on the PSD analysis.

5. CONCLUSIONS

The microstructure, chemistry and corrosion behaviors of Ni-P based alloy coatings on the surface of carbon steel prepared by electroless deposition method have been systematically investigated using SEM, EDX, and electrochemical technique. The results showed that the bath solution chemistry considerably affected the surface morphology of Ni-P coatings formed on the ASTM A615 carbon steel rebar but not as dramatically for Ni-P-Zn coatings. The electrochemical experiments proved that the electroless Ni-P coatings significantly improved the ASTM A588 carbon steel substrate (likely via formation of nano- and micro-crystalline deposits) and led to corrosion behavior nearly comparable to 304 stainless steel coupons. The coatings on the rebar surface also greatly reduced the risk of pitting corrosion and crevice corrosion in the basic and salty environment. Moreover, the carbon steel rebars coated by the Ni-P-Zn featured the highest noise resistance and lowest corrosion rate over the 72-h exposure, followed by the carbon steel rebars coated by the Ni-P and then the 316 stainless steel rebars. The noise data confirm that the Ni-P and Ni-P-Zn coatings greatly enhanced the corrosion resistance of the carbon steel substrate. The Power spectrum density (PSD) data suggest that the corrosion resistance of the carbon steel rebars coated by Ni-P or Ni-P-Zn

coatings fell between that of the bare carbon steel rebars (A615) and that of bare stainless steel rebars (A316). This study lays the groundwork for developing a cost-effective method to protect steel bar for concrete applications. Future work will validate the long-term performance of such coated rebar in concrete specimens exposed to chloride or mechanical loadings, unravel the early-stage corrosion initiation mechanism, and develop new additions such as nano-sized materials into the electroless coating to further enhance the corrosion and abrasion performance of the rebar.

ACKNOWLEDGEMENTS
The authors gratefully acknowledge financial support by the ChuTian Scholar Visiting Professorship Fund provided by the Hubei Department of Education, China; by the U.S. DOT Research and Innovative Technology Administration; and by the National Natural Science Foundation of China (No. 20975002) and the key project of Chinese Ministry of Education.

References

1. S. Ahmad, *Cem. Concr. Res*. 25 (2003) 459-471.
2. X. Shi, Y. Liu, M. Mooney, M. Berry, B. Hubbard, T. A. Nguyen, *Corros. Rev*. 28 (2010) 105-153.
3. X. Shi, T. A. Nguyen, P. Kumar, Y. Liu, *Anti-Corros. Meth. Mater*. 58 (2011) 179-189.
4. Y. Liu, X. Shi, ASCE J. *Mater. Civ. Eng*. (2012), in press. DOI: 10.1061/(ASCE)MT.1943-5533.0000399.
5. H. Yu, X. Shi, W. H. Hartt, B. Lu, *Cem. Concr. Res*. 40 (2010) 1507-1516.
6. Y. Zhao, J. Yu, W. Jin, *Corros. Sci*. 53 (2011) 3388-3397.
7. D.D. Macdonald, M.C.H. Mckubre, M. Urquidimacdonald, *Corrosion* 44 (1988) 2-7.
8. F.J. Molina, C. Alonso, C. Andrade, *Mater. Structures* 26 (1993) 532-548.
9. X. Shi, T. A. Nguyen, Z. Suo, Y. Liu, R. Avci, *Surf. Coat. Technol*. 204 (2009) 237-245.
10. X. Shi, Z. Yang, T. A. Nguyen, Z. Suo, R. Avci, S. Song, *Science in China, Series E: Technological Sciences* 52 (2009) 52: 52-66.
11. H. Xiao, F. Mansfeld, *J. Electrochem. Soc.* 141 (1994) 2332-2337.
12. Z. Abdel Hamid, W. A. Ghanem, S. A. Abo EI Enin, *Surf. Interface Anal*. 37 (2005) 792-796.
13. Y. Liu, X. Shi, *Rev. Chem. Eng*. 25 (2009) 339-388.
14. Y. Liu, X. Shi, *Corros. Rev*. 27 (2009) 53-82.
15. M. Manna, N. Bandyopadhyay, D. Bhattacharjee, *Surf. Coat. Technol*. 202 (2008) 3227–3232.
16. J. Colaruotolo, D. Tramontana, in: G.O. Mallory, J.B. Hajdu (Eds.), Electroless Plating, American Electroplaters' and Surface Finishers Society, 1990, p. 20.
17. R.N. Duncan, *Met. Prog*. 127 (1985) 31.
18. K.S. Rajam, I. Rajagopal, S.R. Rajagopalan, *Met. Finish*. 88 (1990) 77.
19. R.N. Duncan, *Plat. Surf. Finish*. 83 (1996) 65.
20. G.G. Gawrilov, U.K. Redhill, Portcullis Press, 1979.
21. N. Dadvand, W. F. Caley, G. J. Kipouros, Canadian Metallurgical Quarterly 43 (2004) 219-228.
22. J. Flis, D.J. Duquette, *Corrosion* 41 (1985) 700.
23. K. Hladky, J. L. Dawson, *Corros. Sci.* 21 (1981) 317-322.
24. P. C. Searson, J. L. Dawson, *J. Electrochem. Soc*. 135 (1988) 1908-1915.
25. G. Du, J. Li, W. K. Wang, C. Jiang, S. Z. Song, *Corros. Sci*. 53 (2011) 2918-2926.
26. A.Legat, V. Dolecek, *Corrosion* 51 (1995) 295.
27. C. C. Lee, F. Mansfeld, *Corros. Sci*. 40 (1998) 959-962.
28. J. F. Chen, W. F. Bogaerts, *Corros. Sci*. 52 (1996) 753-759.
29. C. A. Loto, R. A. Cottis, *Corrosion* 45 (1989) 136-141.

30. X. Shi, T. A. Nguyen, P. Kumar, Y. Liu, *Anti-Corros. Meth. Mater.* 58 (2011) 179-190.
31. F. Mansfeld, Z. Sun, C. H. Hsu, *Electrochim. Acta* 46 (2001) 3651-3664.
32. A.M. Lafront, W. Zhang, S. Jin, R. Tremblay, D. Dube, E. Ghali, *Electrochim. Acta* 51 (2005) 489-501.
33. B. Zhao, J. H. Li, R. G. Hu, R. G. Du, C. J. Lin, *Electrochim. Acta* 52 (2007) 3976-3984.
34. D. D. N. Singh, R. Ghosh, *Surface & Coating Technology* 201 (2006) 90-101.
35. H. He, Z. Qin, D. W. Shoesmith, *Electrochim. Acta* 56 (2010) 53-60.
36. A.Yabuuchi, M. Maekawa, A. Kawasuso, *J. Nuclear Mater*. 419 (2011) 9-14.
37. Y. Gao, Z. J. Zheng, M. Zhu, C. P. Luo, *Mater. Sci. Eng.* A 381 (2004) 98-103.
38. G. Lu, G. Zangari, *Electrochim. Acta* 47 (2002) 2969-2979.
39. P. Pawar, A. B. Gaikawad, P. P. Patil, *Sci. Technol. Adv. Mater*. 7 (2006) 732-744.
40. Y. Subbaiah, V. Kaje, A. C. Hegde, *Anti-corros. Meth. Mater*. 58 (2011) 84 – 89.
41. F. Mansfeld, Z. Sun, C. H. Hsu, A. Nagiub, *Corros. Sci*. 43 (2001) 341-352.
42. A.Nagiub, F. Mansfeld, *Electrochim. Acta* 47 (2002) 2319-2333.
43. J. C. Uruchurtu, J. L. Dawson, *Corrosion* 43 (1987) 19-25.

Table S1. Surface chemical composition of bare and coated steel coupons, determined by EDX (wt%).

Sample	Fe	Ni	P	Zn	S	Ni/Fe	P/Ni
Uncoated A588	93.9	0.10	0.15	0.18	0.06	0.001	1.5
Ni-P (#P2)	0.24	87.46	6.55	0.00	0.00	364	0.075
Ni-P (#P3)	0.28	89.01	4.84	0.00	0.09	318	0.054
Ni-P-Zn (#P4)	85.22	9.05	0.53	0.27	-	0.106	0.058


Control (bare A615 carbon steel)


Control (304 stainless steel)


Good Ni-P coating (#P2)

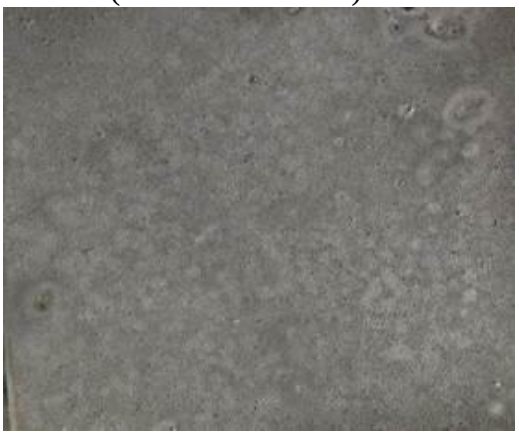
Poor Ni-P coating (#P3)

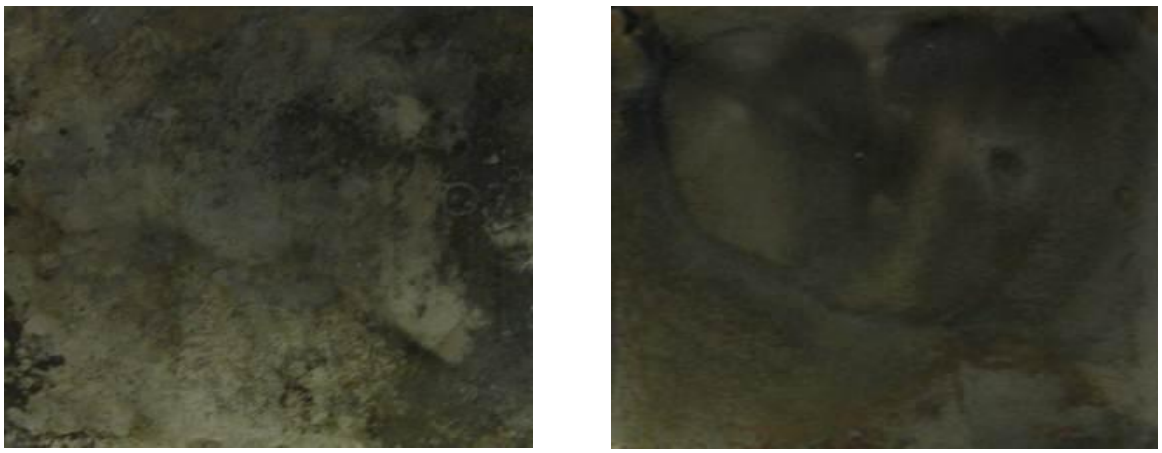

Worse Ni-P coating (#P1) Worst Ni-P-Zn coating (#P4)

Figure S1. Example digital photos of bare and coated steel rebar surfaces.

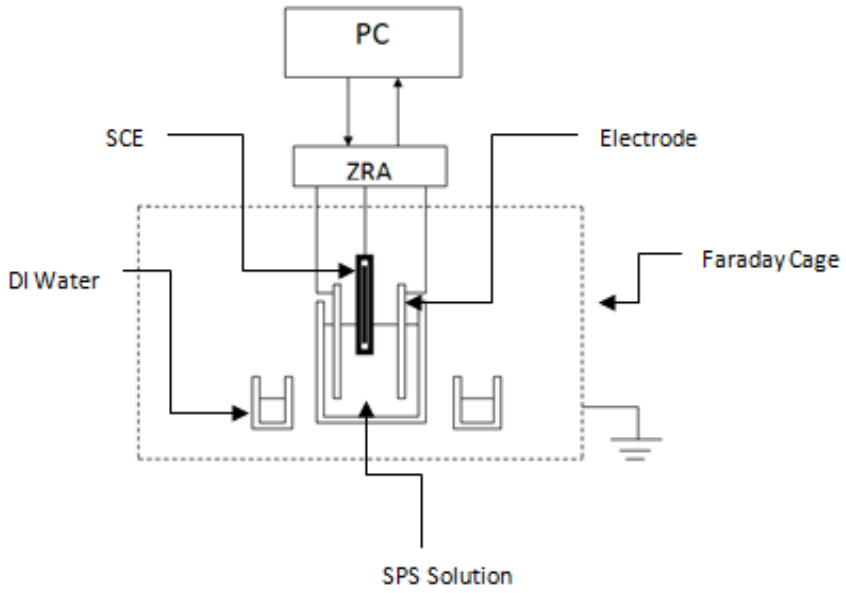

Figure S2. Experiment setup for electrochemical noise measurements.